6. Analysis

6.1. Event Selection

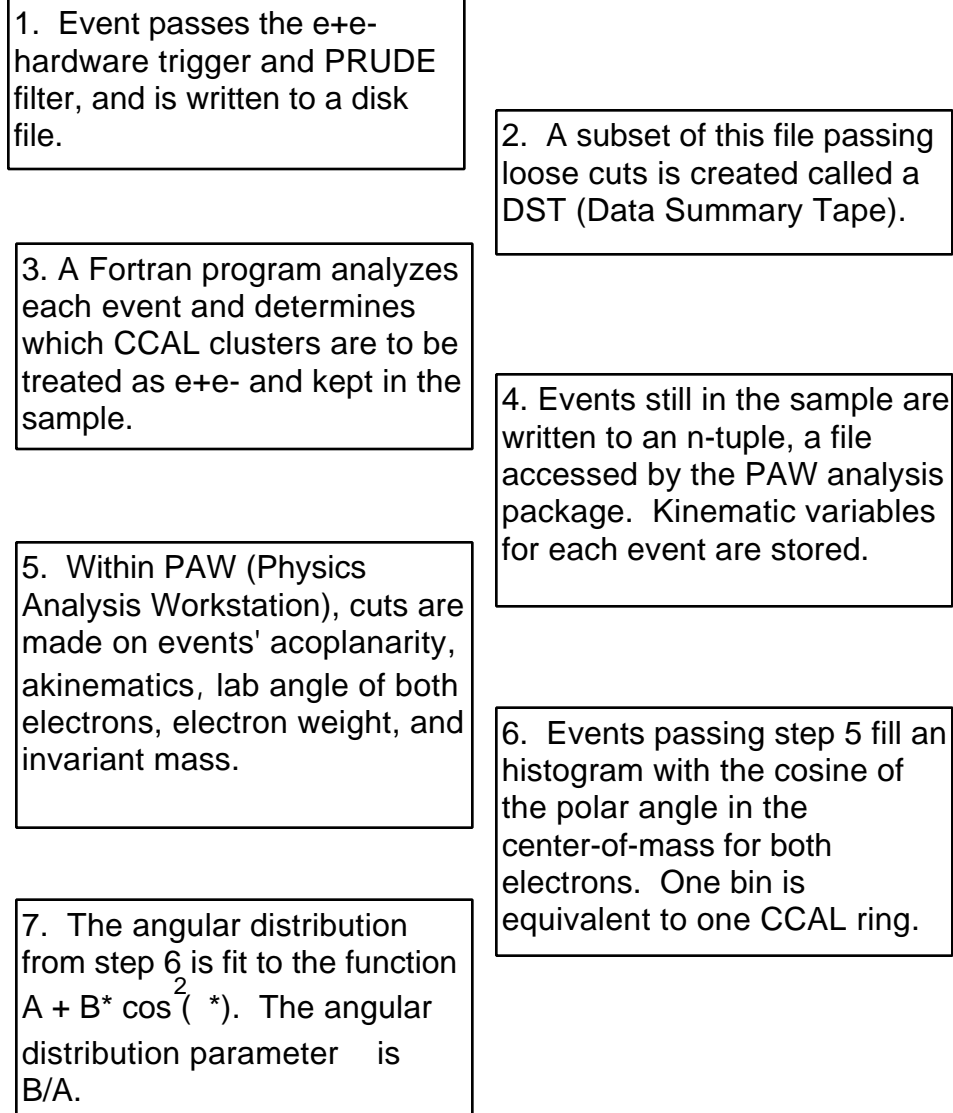1. Event passes the e+e- hardware trigger and PRUDE filter, and is written to a disk file.

2. A subset of this file passing loose cuts is created called a DST (Data Summary Tape).

3. A Fortran program analyzes each event and determines which CCAL clusters are to be treated as e+e- and kept in the sample.

4. Events still in the sample are written to an n-tuple, a file accessed by the PAW analysis package. Kinematic variables for each event are stored.

5. Within PAW (Physics Analysis Workstation), cuts are made on events' acoplanarity, akinematics, lab angle of both electrons, electron weight, and invariant mass.

6. Events passing step 5 fill an histogram with the cosine of the polar angle in the center-of-mass for both electrons. One bin is equivalent to one CCAL ring.

7. The angular distribution from step 6 is fit to the function $A + B* \cos^2(\theta*)$. The angular distribution parameter λ is B/A.

Figure 6.1 : Data Analysis Flow Chart.

Initially, events that pass the hardware e$^+$e$^-$ trigger are reconstructed by the PRUDE filter and written to disk. From these resident disk files, loose cuts

are applied in order to produce a DST file, also residing on disk. A *Data Summary Tape* (DST) file is a subset of all the events in the disk file that does not include the large hadronic background present below 2.7 GeV. The event is rejected if (a) the event did not fire Gatemaster bit 1 (the e^+e^- trigger), (b) the number of clusters seen by the central calorimeter is greater than 20, or (c) the largest possible invariant pair mass constructed from a cluster pair is less than 2.7 GeV.

For this analysis, cluster thresholds were set at 25 MeV for the seed block of the cluster, and 25 MeV for the entire cluster. When a particle such as an electron enters the CCAL, it creates an electromagnetic shower which produces Cerenkov light in several neighboring lead glass blocks. The amount of Cerenkov light is proportional to the amount of energy deposited in each block. A software program called the clusterizer searches for possible "seed" blocks, around which the energy deposits are grouped into clusters. A cluster is the CCAL's representation of the particle that entered it. A cluster pair is defined to be "on-time" if the TDC values (which flag the cluster creation with respect to the time the interaction occurred) of its largest energy deposits are on-time.

From the smaller DST file, further cuts are applied to the data to establish the thesis sample and event information is written to an n-tuple, a file that stores processed information for future use within PAW (Physics Analysis Workstation analysis package). A typical n-tuple may hold the values of 25 to 30 kinematic

variables for each event. If the on-time cluster pair that generates the invariant

mass closest to the resonance in question is greater than 2.0 GeV, then the

information for that event is written to the n-tuple.   Note that we did not require

that the largest invariant pair mass had to be on-time for the event to be

included on the DST. The on-time cluster pair yielding the closest invariant

mass to the resonance is chosen to be the e^+e^- pair, although there is no way to

tell which cluster is the positron and which is the electron.

At this juncture the thesis sample is refined using the PAW analysis

package. For example, suppose one wants to plot the invariant mass of all the

events in the n-tuple with only 2 on-time clusters.   "kumac" files may include a

large list of commands like those below, and allow Fortran programs to be

called from within PAW to analyze the data. The general procedure is as

follows:


```
> pawX11                              ! Launch the PAW software
                                      ! package.
>hi/file 1 /scratchj/mctaggar/jpsi.ntp    ! Load the desired n-tuple.
>ntuple/plot 20.s12 ontime.eq.2       ! Display an histogram of the
                                      ! invariant mass (s12) of all
                                      ! events  whose value
                                      ! of "ontime" is 2.
```

79

To obtain the angular distribution of the final e$^+$e$^-$ state, several cuts are applied to the data. In the case of the J/ψ, the event must first have an invariant mass greater than 2.7 GeV (Figure 6.1). For the ψ', it must have an invariant mass greater than 3.4 GeV (Figure 6.2). The latter cut removes most of the decays of the ψ' to J/ψ + X, where X may be either 2π or simply an η. Here the two electrons result from the cascading decay of the J/ψ instead of the exclusive decay of the ψ'. The resonance below the J/ψ, the η$_c$, is not allowed to decay to e$^+$e$^-$ by parity, so this additional inclusive channel is not present for the J/ψ sample. The distributions shown in Figures 6.2 and 6.3 demonstrate the mass resolution of the central calorimeter.
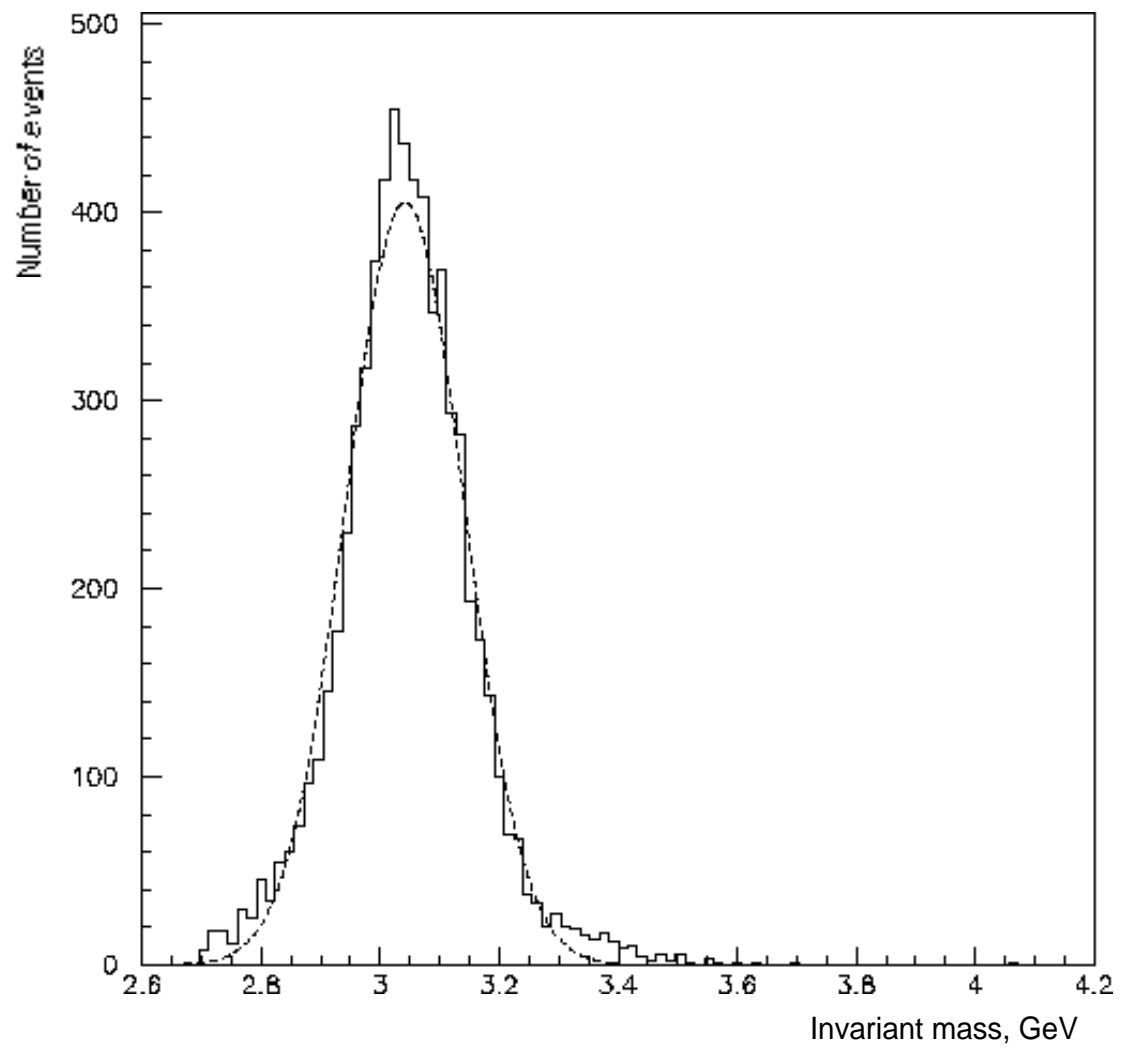
Figure 6.2 : Invariant mass of the J/ψ thesis sample.
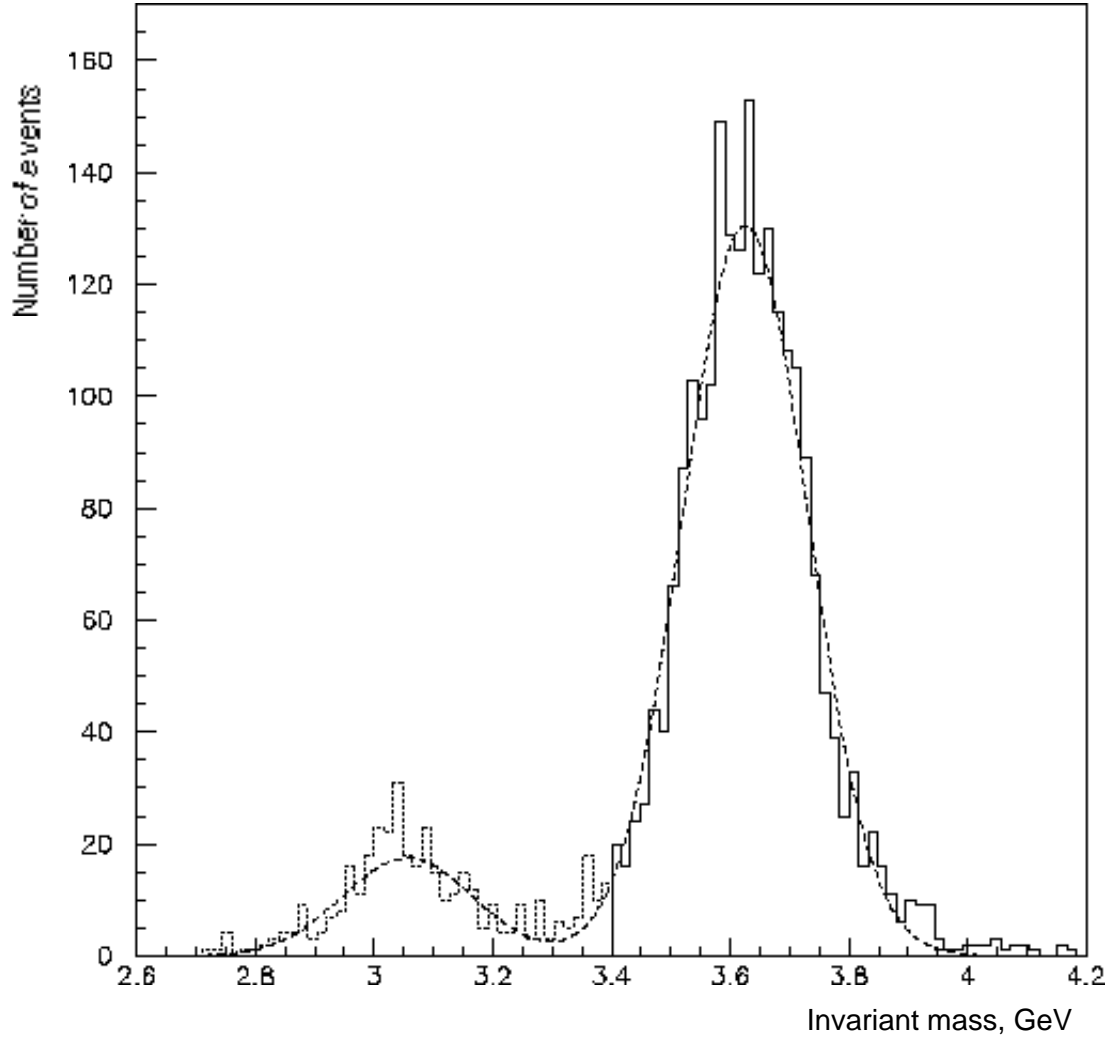
Figure 6.3 : Invariant mass of the   ' thesis sample.

Second, events are removed if their acoplanarity and akinematics are too large.   In the center-of-mass frame, the electrons from an exclusive charmonium decay should come out back-to-back. Zero acoplanarity means the event is exactly back-to-back in terms of the azimuthal angle. Zero akinematics means the event is perfectly back-to-back in terms of the center-of-mass polar angle. In practice, both quantities have a distribution centered on

zero for pure e⁺e⁻ events due to the resolution of the central calorimeter. The distributions for the acoplanarity and akinematics of all events residing in the n-tuple are shown in Figures 6.4-6.7 (all of the abscissa are in units of radians). If the event's acoplanarity or akinematics is greater than 25 milliradians, the event does not contribute to the angular distribution.
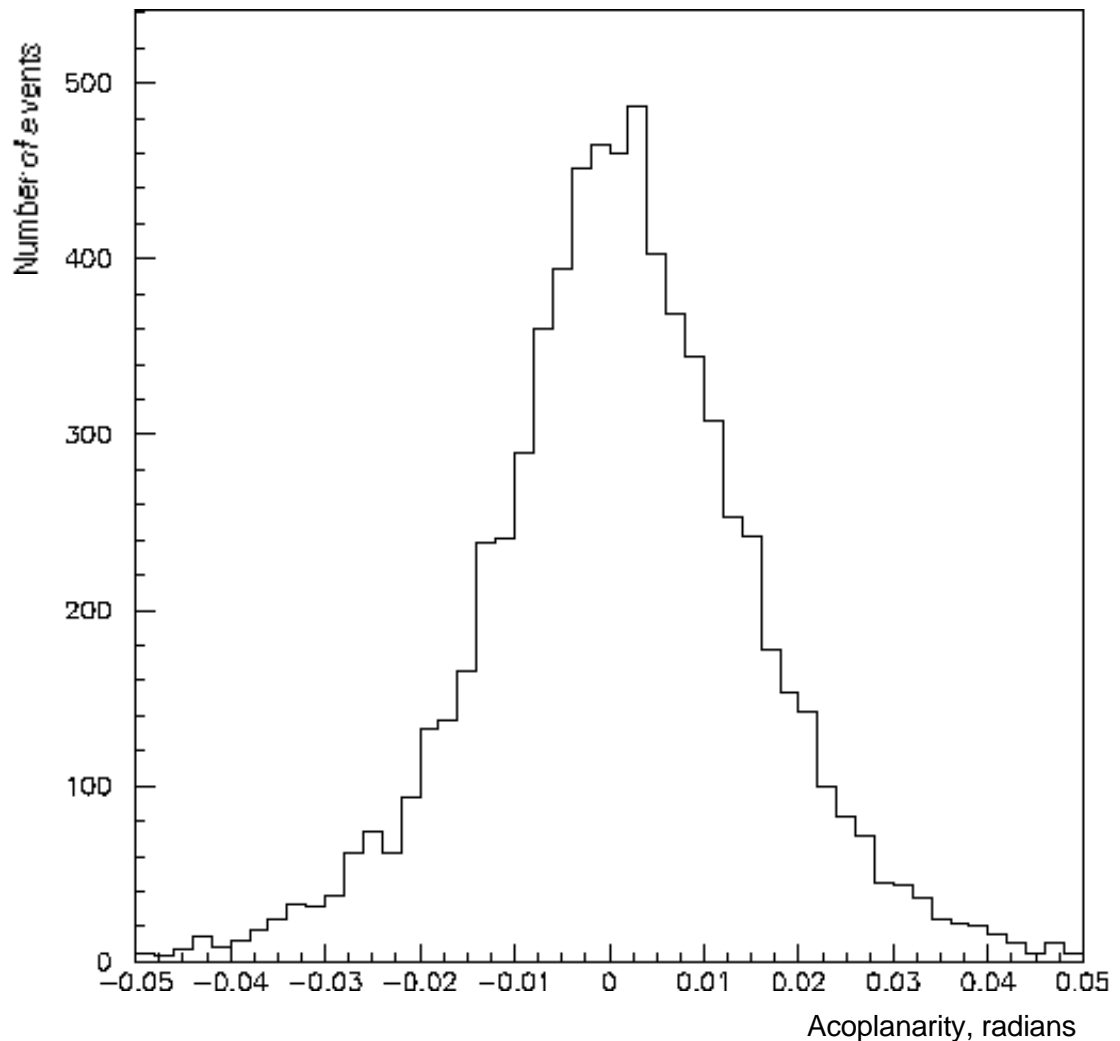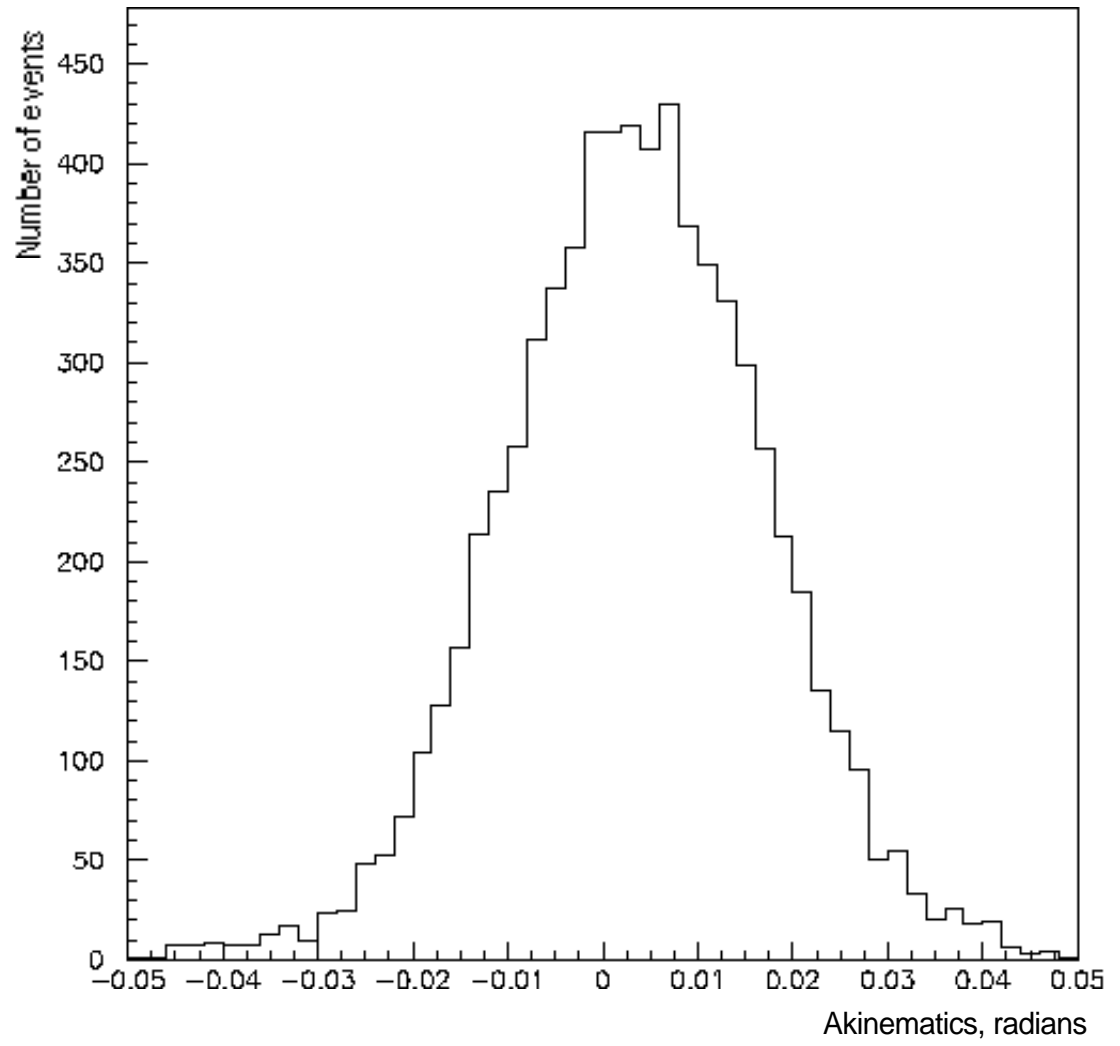

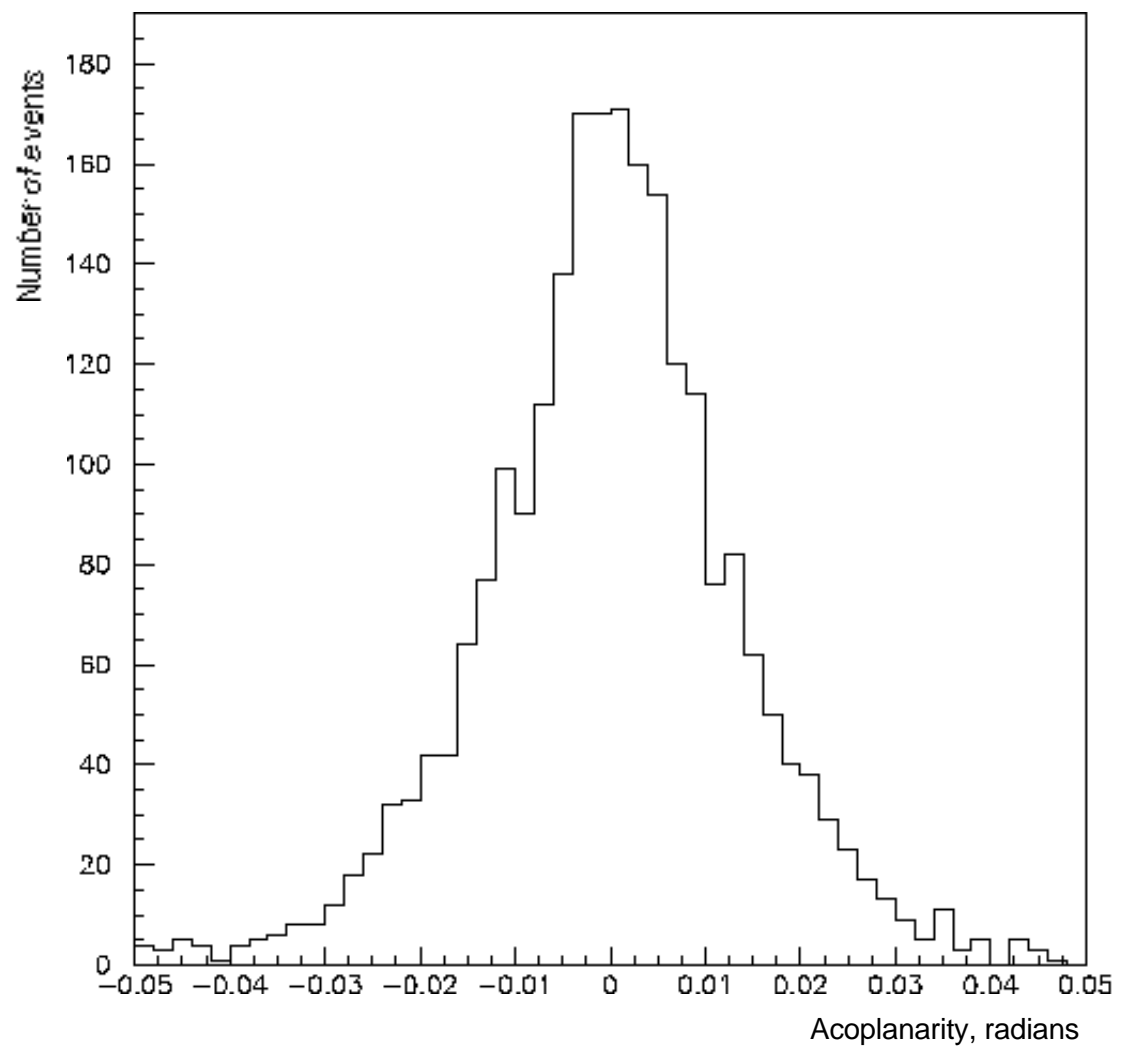Figure 6.4 : J/ Acoplanarity.

Figure 6.5 : J/ψ Akinematics.
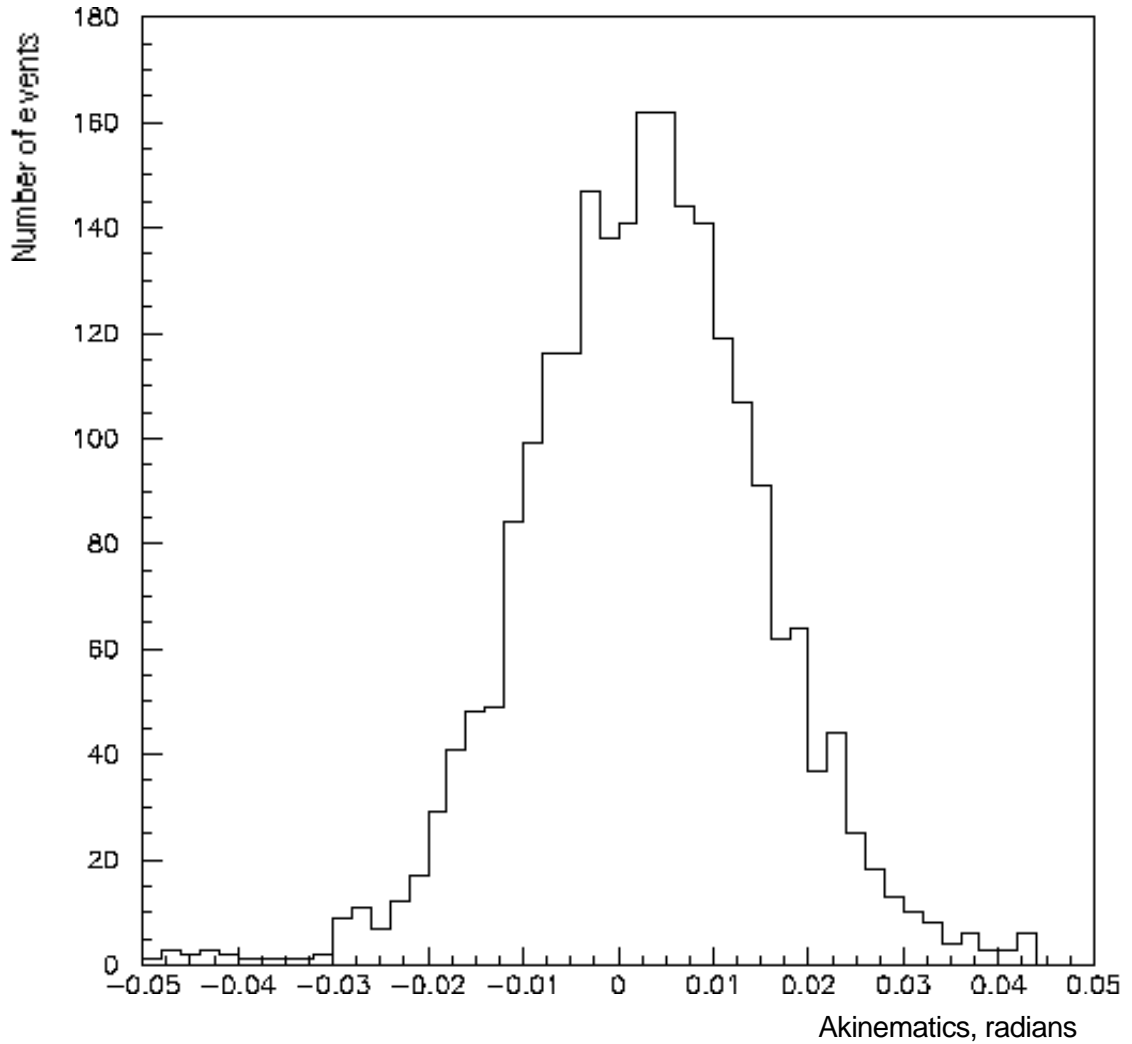
Figure 6.6 :   ' Acoplanarity.

85

Figure 6.7 :   ' Akinematics.

Third, the polar lab angles of both electrons must lie between 15 and 60

degrees in the lab frame, as determined by the offline CCAL clusterizer. As a

result, both electrons must pass through the acceptance of the inner

detectors(and hopefully leave a charged track). Clusters produced in this range

should also be fully contained within the CCAL. Reducing the polar angle limit

of 15 degrees implies dealing with the higher cross-sections for multi-pion

channels and beam-pipe interactions in the forward direction. The forward
calorimeter is thus not used in this analysis.

Finally, an "electron weight" cut (see Table 6.1) is applied. Each cluster
in the central calorimeter is assigned a composite probability called the electron
weight , which uses the following information from the inner detectors and the
central calorimeter to compare the likelihood ratio of an "electron" hypothesis
with a "background" hypothesis[92]: dE/dx in all three hodoscopes (H1, H2, H2'),
the Cerenkov pulse height (which may vary from mirror to mirror), second
moments of the energy along both rings and wedges (on a 3 by 3 grid), the ratio
of energy in a 3 by 3 grid to that in a 5 by 5 grid centered on the highest energy
block in the cluster, the ratio of the energy in a 2 by 2 grid (for the two blocks
with the largest energy) to that in the surrounding 4 by 4 grid, and the invariant
mass of the cluster. The product of the electron weights for each cluster pair is
then related to the probability that the cluster pair is in reality due to e^+e^-.

dE/dx in all hodoscopes.
Cerenkov pulse height.
Second moments of the energy.
3 X 3 / 5 X 5 energy ratio.
2 X 2 / 4 X 4 energy ratio
Cluster invariant mass.
Comparison of electron and background hypotheses.

Table 6.1 : Components of the Electron Weight.

In this analysis, an electron weight product of greater than 0.1 is applied to the data. The electron weight is useful in weeding out clusters created by charged pions, which do not shower in the CCAL like electrons do, and they in general can be separated from the electrons by the Cerenkov pulse height. Neutral pions will decay into photons, and will not generate charged tracks like electrons do. The inner detectors cannot contribute to the electron weight outside of the fiducial polar lab angle described above, and in fact there is some inefficiency near the edges of this acceptance.

The effects of each of these cuts on an uncorrected data sample are shown in Tables 6.2 and 6.3 respectively for the J/ and the '. The first column is the number of events in the n-tuple passing all the above mentioned

cuts except the cut in that row. The total number of events passing all cuts is not the total number of entries included in the final fit: The sample first undergoes a smoothing procedure, a correction for the geometrical efficiency, and then a range in cos(*) is selected for the final fitting of the angular distribution.

Applied Cut	Event Count	Efficiency
Electron Weight (ELW)	9018	72.6 %
Acoplanarity (acopl)	8488	77.1 %
Akinematics (akin)	8679	75.4 %
Fiducial Lab Angle	8370	78.2 %
ELW, acopl	7985	82.0 %
ELW, akin	8184	80.0%
ELW, lab angle	7956	82.3 %
acopl, akin	7752	84.4 %
acopl, lab angle	7377	88.7 %
akin, lab angle	7481	87.5 %
ELW, acopl, akin	7346	89.1 %
ELW, acopl, lab angle	7110	92.0 %
ELW, akin, lab angle	7230	90.5 %
acopl, akin, lab angle	6758	96.9 %
ELW, acopl, akin, lab angle	6546	100 %

Table 6.2: Effect of different cuts on the J/ψ event sample. "Efficiency" is a comparison with all cuts applied.

Applied Cut	Event Count	Efficiency
Electron Weight (ELW)	2856	76.7 %
Acoplanarity (acopl)	2920	75.0 %
Akinematics (akin)	3052	71.8 %
Fiducial Lab Angle	3316	66.0 %
ELW, acopl	2451	89.4 %
ELW, akin	2547	86.0 %
ELW, lab angle	2686	81.5 %
acopl, akin	2644	82.8 %
acopl, lab angle	2631	83.2 %
akin, lab angle	2702	81.1 %
ELW, acopl, akin	2309	94.8 %
ELW,acopl, lab angle	2325	94.2 %
ELW, akin, lab angle	2396	91.4 %
acopl, akin, lab angle	2404	91.1 %
ELW, acopl, akin, lab angle	2190	100 %

Table 6.3: Effect of different cuts on the   ' event sample. "Efficiency" is a comparison with all cuts applied.

6.2. Background to the Event Sample

Two different sets of runs used in the search of the elusive η_c' (2^1S_0) are used to determine the amount of background present in the data from the e^+e^- continuum: Runs 1283-1289 were taken at 3576 MeV, and runs 1180-1184 were taken at 3660 MeV. The quantum numbers of the η_c' do not permit it to decay directly to e^+e^-, and below the threshold for OZI-allowed decays only the J/ψ and the ψ' are allowed to do so.

Both sets of data went through the same analysis flow chart shown in Figure 6.1, with the centers of mass were given as 3576 MeV and 3660 MeV respectively. However, equal-sized bins are used here. Thus the clusters representing the background candidates were a) on-time and b) had the invariant mass closest to the center of mass. The results are applied to both the J/ψ and the ψ'.

The invariant mass distributions of the background candidates passing step 4 in Figure 6.1 are presented in Figure 6.8 for the set at 3576 MeV and in Figure 6.9 for set at 3660 MeV. The rationale for cutting events with an invariant mass of less than 2.7 GeV can clearly be seen in both of these figures: The background without any cuts increases rapidly below this threshold. After applying all the analysis cuts, very few events remain, as one can see in Table

6.4, Figure 6.10 for the 3576 MeV runs, and Figure 6.11 for the 3660 MeV runs.

Background Point	Number of events present in n-tuple	Background candidates
3576 MeV	4180	4
3660 MeV	4697	4

Table 6.4 : Background estimate from off-resonance data.

The angular distribution of the background candidates are shown in Figures 6.12 and 6.13. Both leptons from each event contribute to the event. After all of the cuts, one is left with Figures 6.14 and 6.15. Two attributes of these graphs need to be addressed. First the background candidates, originating from multi-pion events and beam-pipe interactions, are forward-peaked. The cuts do an excellent job in removing these events. Second, one sees an oscillation in the angular distribution due to a bias in the clusterizer when many equal-sized bins are used. This subject is addressed in Section 6.3.

A secondary source of background arises for the (3686) because it may decay to the J/ (3097) via another channel, for example the 2 channel (an inclusive decay as opposed to an exclusive decay). The e^+e^- pair found by the

analysis may in fact have come from the decay of the J/ψ.

In the invariant mass plot of Figure 6.3, one can clearly see 2 different contributions. The smaller bump on the left near 3.1 GeV is due to the inclusive decay of the ψ' to the J/ψ, and the larger bump near 3.6 GeV is due to the exclusive decay to e^+e^- that is the focus of this thesis. The amount of contamination from the inclusive decays is small, especially with the mass cut of 3.4 GeV for the ψ' analysis.
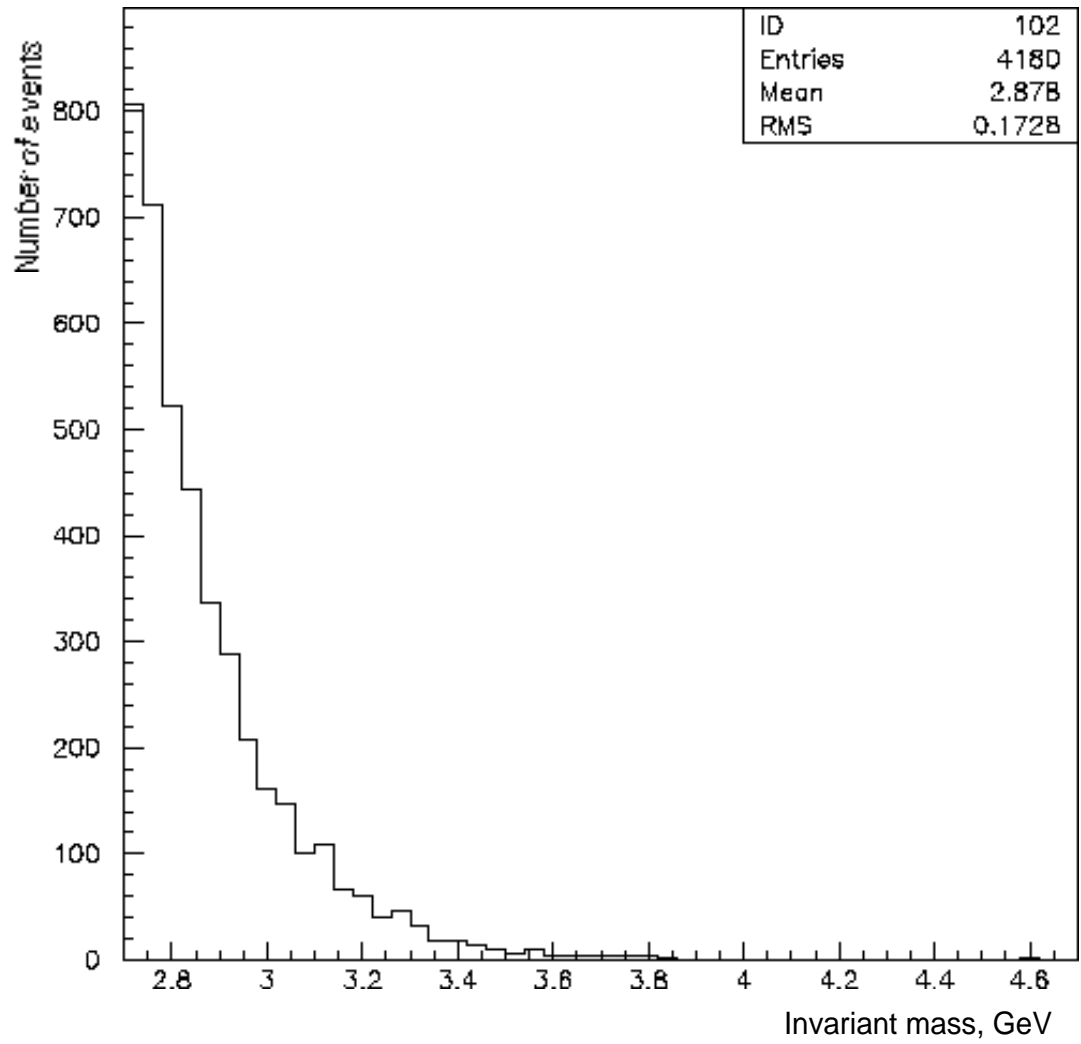
Figure 6.8 : Invariant mass distribution of background before cuts, 3576 MeV.
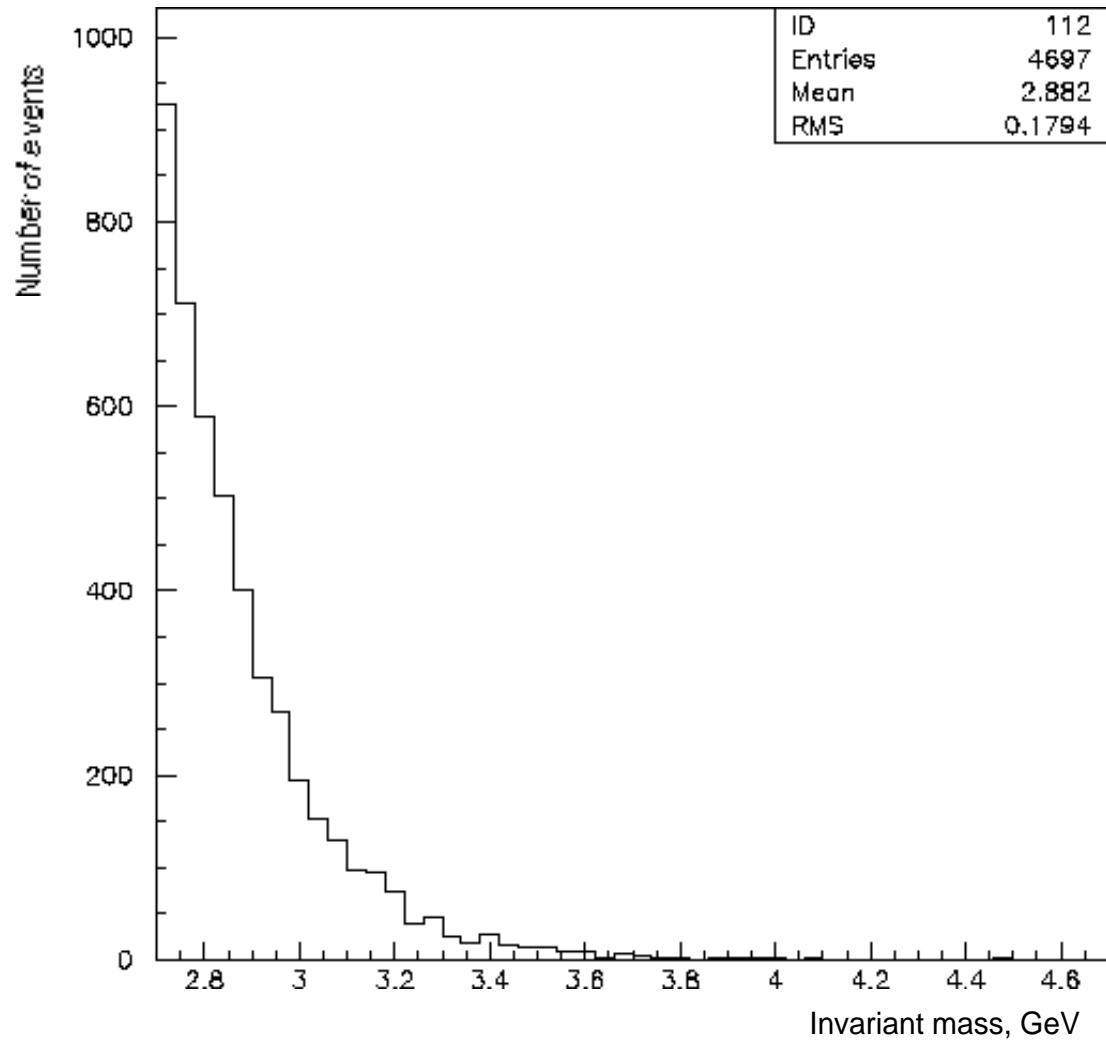
Figure 6.9 : Invariant mass distribution of background before cuts, 3660 MeV.
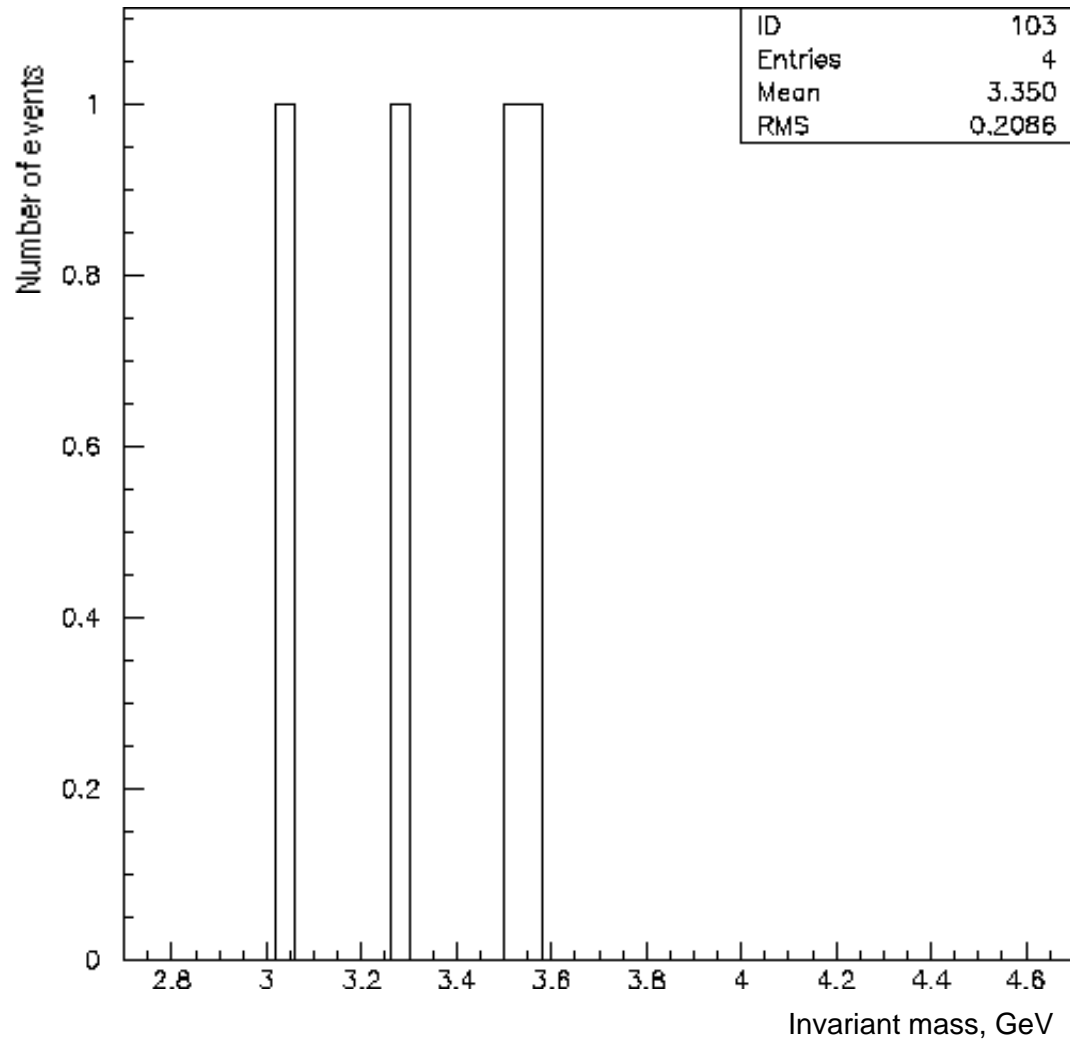
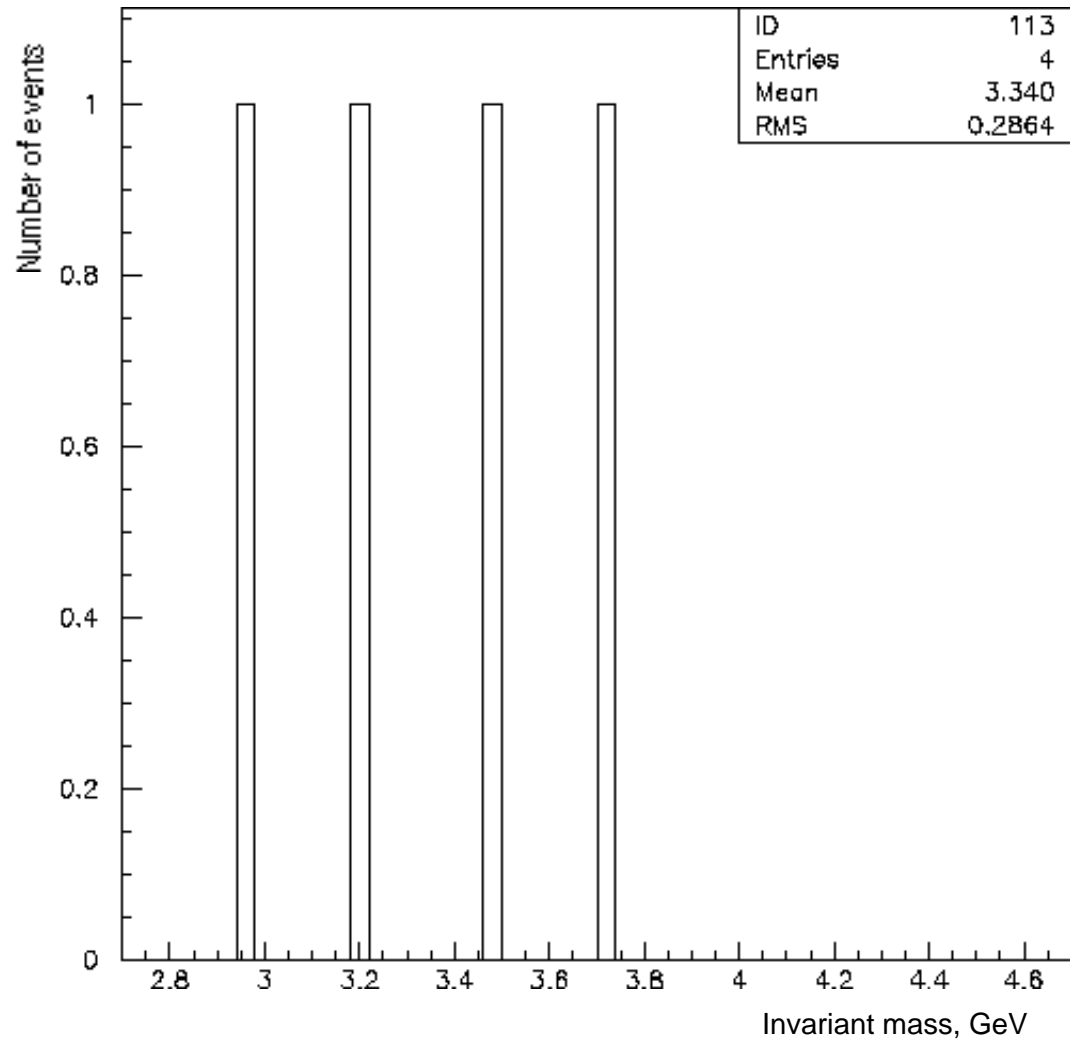Figure 6.10 : Background estimate at 3576 MeV.
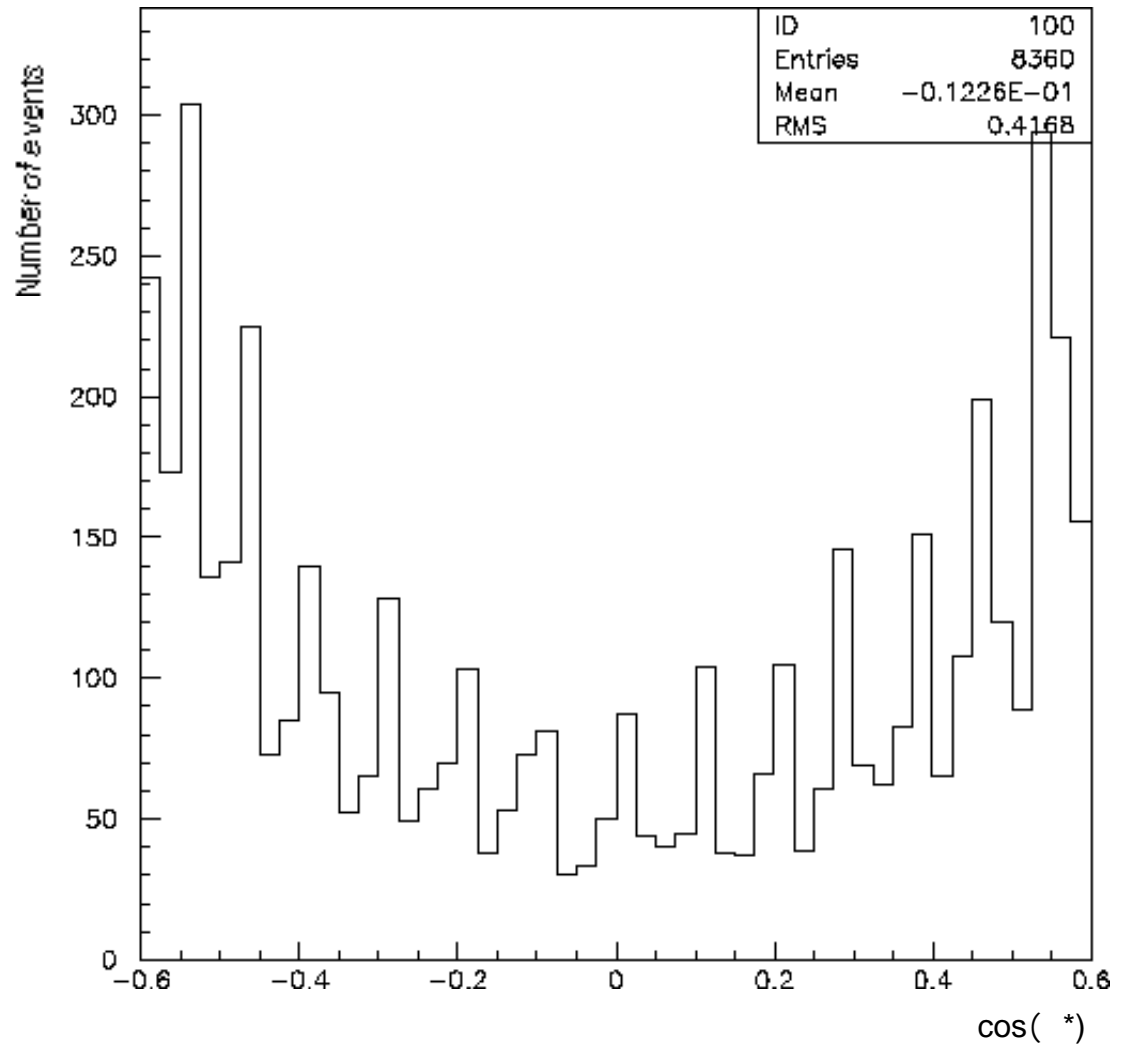
Figure 6.11 : Background estimate at 3660 MeV.

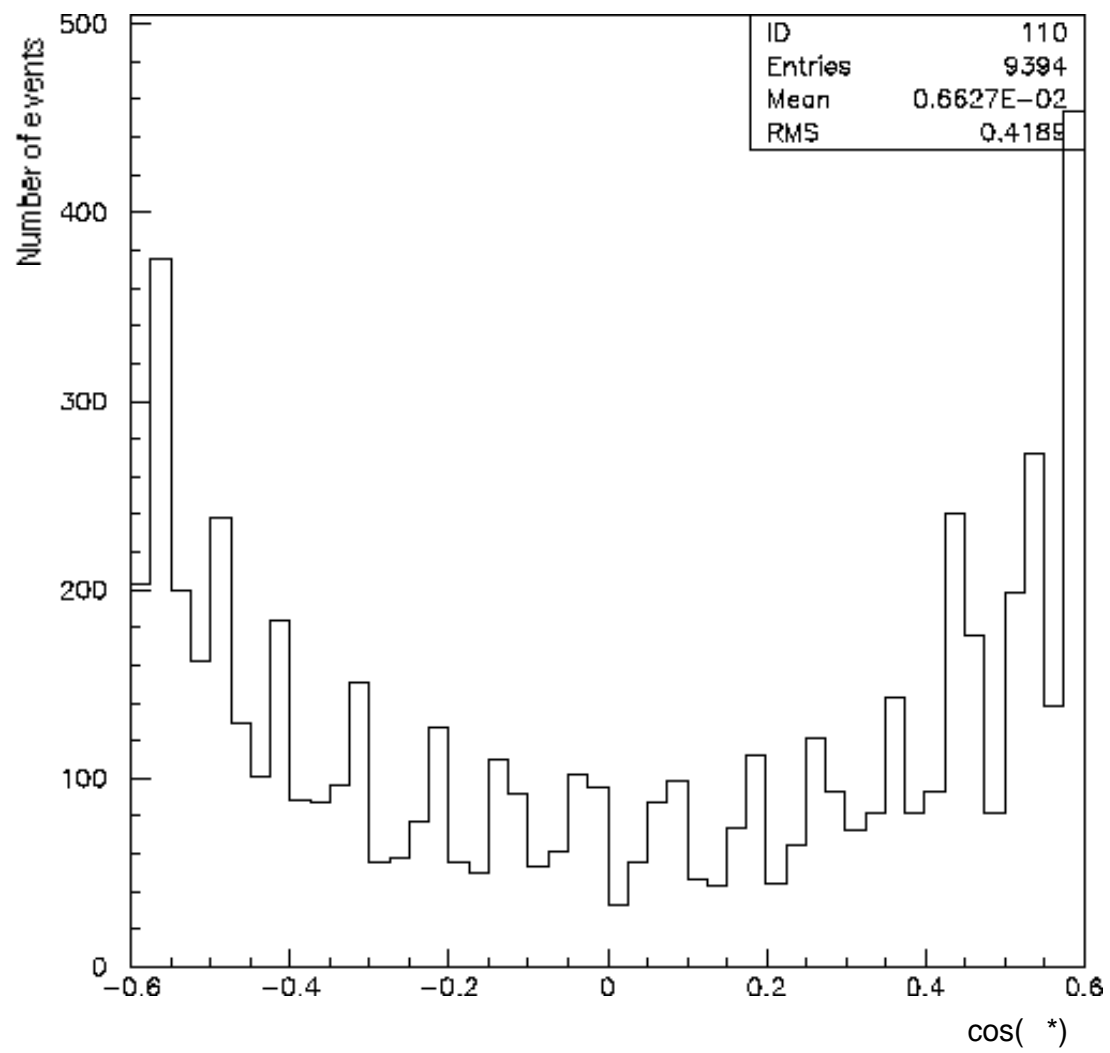Figure 6.12 : Angular distribution of background before cuts, 3576 MeV.

Figure 6.13 : Angular distribution of background before cuts, 3660 MeV.
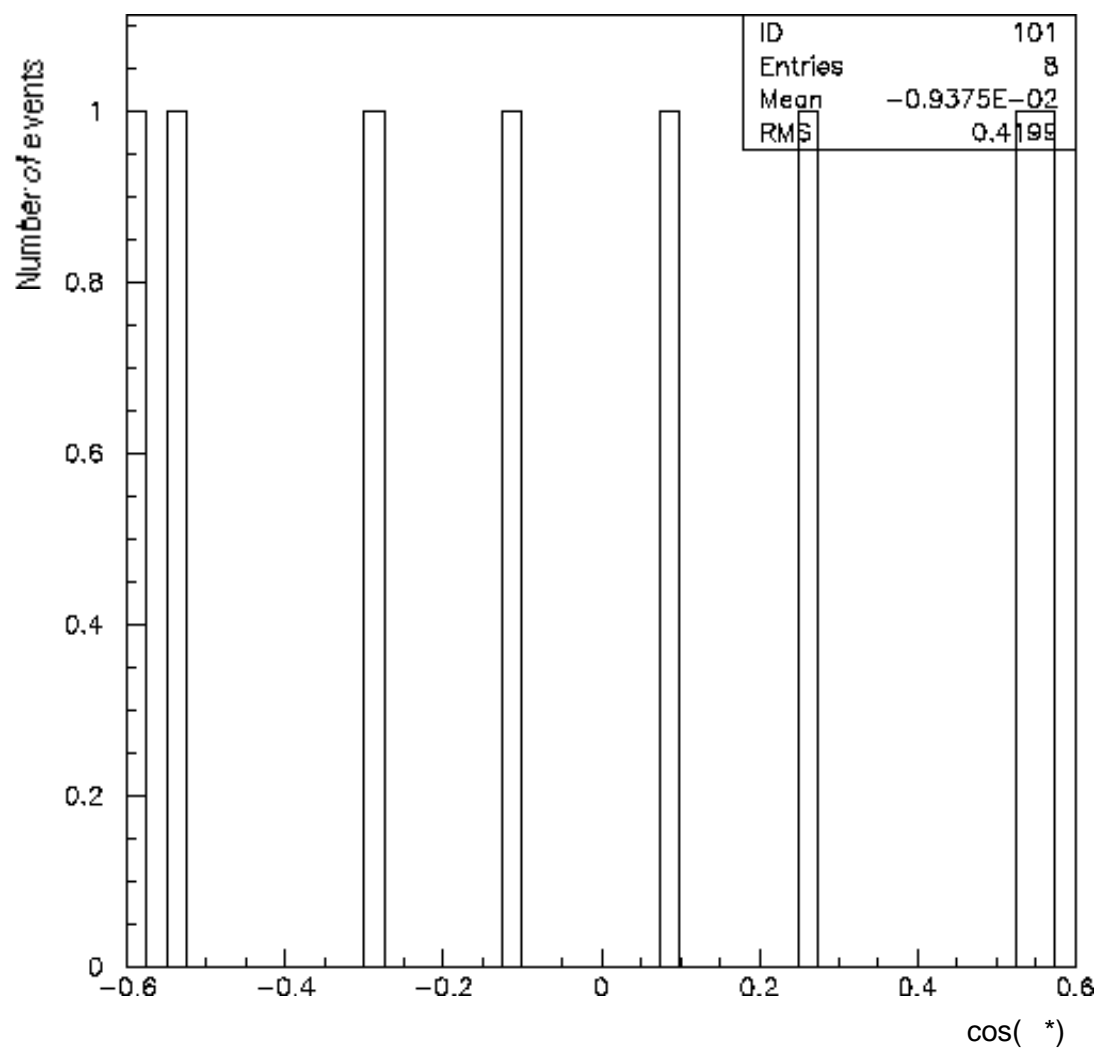
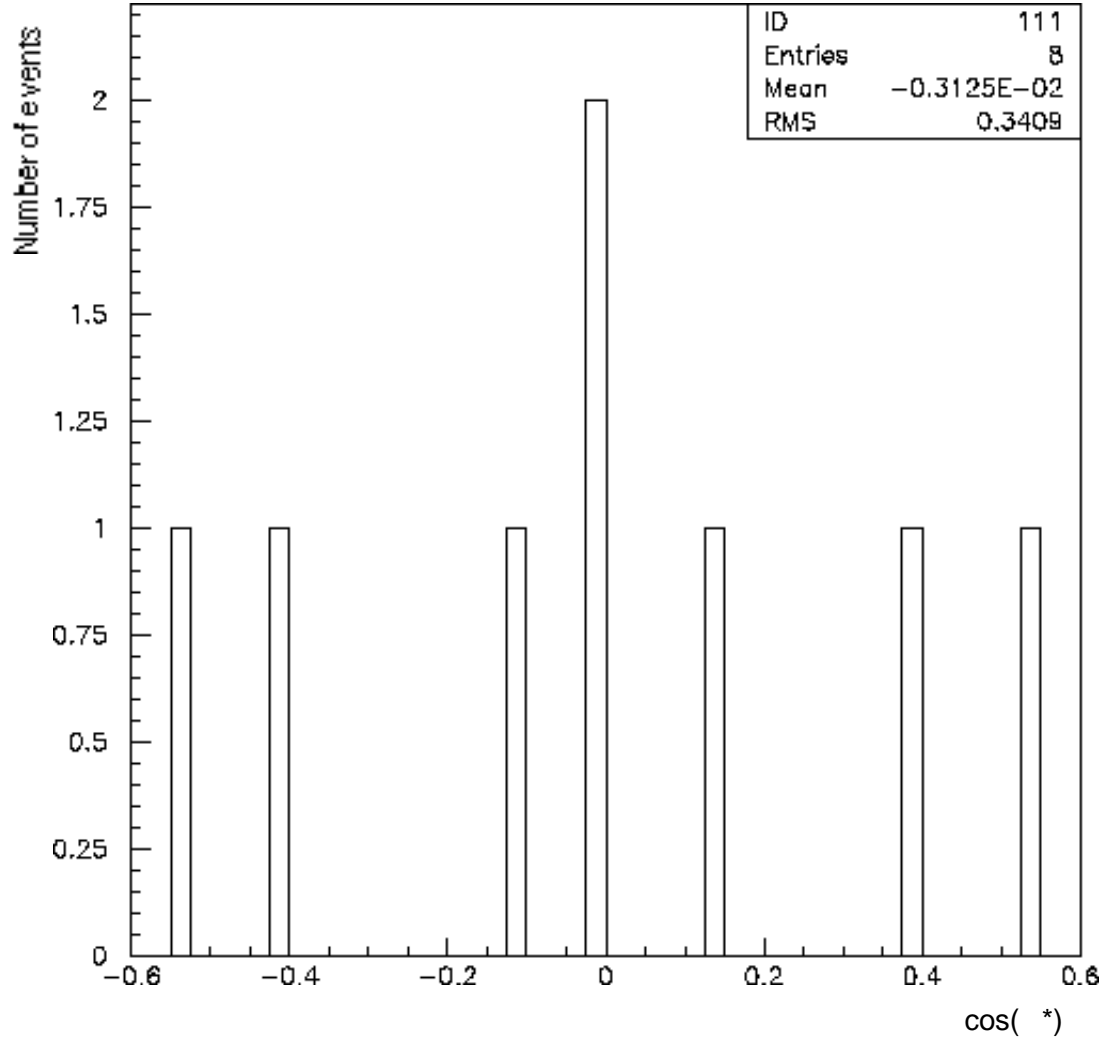Figure 6.14 : Angular distribution of background, 3576 MeV.

Figure 6.15 : Angular distribution of background, 3660 MeV.

6.3. Impact of the CCAL Clusterizer

In reconstructing final e^+e^- states, the present offline clusterizer has a preference for centering clusters across the face of a calorimeter block: Away from block centers and toward the block edges. This results in a modulation of the angular distribution of the e^+e^- in $\cos(\theta^*)$. The primary reason for this

102

behavior is that the resolution of the calorimeter is better near the edges of the

blocks(where 2 photomultiplier tubes can see the event) than at the center

(where only one will receive the energy deposit).

The clusterizer is also better equipped to handle the 2 photon decays of

resonances like the $_2$ or the $_c$ than the e^+e^- decays studied here. Its

algorithms search for energy deposits to group into clusters, and along with the

e^+e^- in the event may come delta rays from the interaction of the electrons with

the detectors. The position of the cluster can be affected by these delta rays that

get absorbed in the clusterizing process.

The result is an unnaturally high chi-square per degree of freedom for the

angular distribution due to the oscillation. There are several ways to address

this oscillation. First, one can take into account the angular resolution of the

calorimeter (studied in E760), convolute the theoretical angular distribution with

the error function and fit the distribution using a maximum likelihood procedure.

Second, one may apply a Gaussian smearing technique based upon the

resolution of the CCAL. Third, one may use the angular information from the

scintillating fibers. Scintillating fibers are a new and exciting technology, but

their efficiencies are not yet understood well enough for this thesis.

None of these were applied to the data. Instead, the histogram for the

angular distribution has been defined using variable-sized bins, where one bin is specifically assigned to each ring. The preparation of this histogram is described below.

6.4. Location of CCAL Rings in the Center-of-Mass Frame

It is assumed that the bias of the clusterizer affects the cluster location within one block face. To remove this affect, the size of each bin should correspond to the polar angular coverage of one ring.

Within the e835 offline, the cluster location is also defined in terms of ring and wedge units. For example, 4 ring units places the cluster in the center of ring 4, and 3.5 or 4.5 places it at one of the edges of ring 4. Determining the locations of each ring edge means finding the corresponding values of cos(*).

The locations of the ring edges are extracted from the data in the following manner. For both electrons simultaneously, a plot of cluster location in terms of ring units versus the corresponding value of cos(*) is made about one edge. For example, if one wants to find the corresponding cosine for the edge between rings 6 and 7 (6.5 in ring units), then both electrons must lie within 6.4 and 6.6 ring units. The location of 6.5 ring units is then obtained visually from the graph.

104

Edge in Ring Units	cos(*), J/	cos(*), '
2.5	-.482	-.625
3.5	-.401	-.561
4.5	-.315	-.489
5.5	-.222	-.409
6.5	-.125	-.323
7.5	-.025	-.230
8.5	.075	-.133
9.5	.174	-.033
10.5	.270	.068
11.5	.361	.167
12.5	.446	.263
13.5		.355
14.5		.440
15.5		.518
16.5		.588

Table 6.4 : Location of CCAL ring edges in the center of mass.

6.5. Corrections to the Angular Distribution

There are two corrections applied to the data. First, there are two dead

spots in the CCAL. No clusters are found in the blocks referenced by (a) ring 7

and wedge 12, and (b) ring 8 and wedge 19. After the correction for the dead

blocks is performed, the angular distribution is adjusted for the varying bin

width. The same blocks affect both the J/ψ and the ψ', and one dead area does

not affect the correction for the other dead region.

The angular distribution is not only affected where the dead blocks occur,

but also where the corresponding lepton would have hit. The shape of this

missing distribution comes from the contribution of the 2 neighboring blocks that

share the same ring as the dead block. The number of events that should have

hit each of the dead blocks is found by averaging the contents of the 8

surrounding blocks, which form a 3 X 3 grid centered on the dead block. The

histogram that is added to the uncorrected angular distribution has the correct

shape, and twice the number of events found from the averaging.

No correction for any inefficiency due to the geometry of the CCAL with a

Monte Carlo[93] has been made. This efficiency is constant and close to one in

the region being fit.

6.6. Polar Angle Dependence of the Electron Trigger

Another possible source of inefficiency which could effect the shape of

the angular distribution may come from a polar angle dependence of the

electron trigger. The electron trigger is made up of the following trigger requests: CMLU(1)*PBG3 + CMLU(2), where CMLU(1) is 2e*(H2<6) + 1e*2h(H2=2)*COPL , and CMLU(2) is 2e*(H2=2)*COPL*(Veto on FCH), and PBG3 is the 1 to 3 back-to-back super-cluster requirement.

The efficiency of the charged trigger (CMLU(1)) was examined during a special trigger run in April of 1997[94], in which data were taken by replacing the 2-electron trigger (2e) with a 1-electron trigger (1e) in order to determine the efficiency of detecting an electron. However, the statistics were too limited to conclude that there was any polar angle dependence. Such a dependence might arise if there were a degradation of the hodoscopes along the z-axis (perhaps a result of radiation damage near the interaction point), but this was not visible. Above and beyond the azimuthal inefficiency brought about by cracks between the elements of the H1 hodoscope, the data taken during this trigger run was consistent with having no azimuthal dependence either. Since the efficiency of the electron trigger is considered to be flat in the center of mass frame, it will not affect the shape of the angular distribution. As a result, the data is not corrected for any polar angle dependence of the electron trigger.

CMLU(1)	Output 1 of the Charged Memory Lookup Unit
CMLU(2)	Output 2 of the Charged Memory Lookup Unit
PBG1	Super-clusters of "electrons" are directly opposite each other.
PBG3	The other "electron" is in one of the 3 opposing super-clusters
1e	At least one Cerenkov cell has a charged track through it.
2e	At least two Cerenkov cells have charged tracks through them.
H2=2	Only 2 of the 32 H2 elements are hit.
H2<6	Less than 6 of the 32 H2 elements are hit.
COPL	2 H2 elements are coplanar.
FCH	More than one forward hodoscope is hit.

Table 6.5 : Definitions for the E835 e^+e^- trigger.